AGU PUBLICATIONS

Supporting Information for "Identifying efficient ensemble perturbations for initializing subseasonal-to-seasonal prediction"

Jonathan Demaeyer[1], Stephen G. Penny[2,3], and Stéphane Vannitsem[1]

[1]Royal Meteorological Institute of Belgium, Brussels, Belgium

[2]Cooperative Institute for Research in Environmental Sciences, University of Colorado Boulder

[3]NOAA Physical Sciences Laboratory, Boulder, Colorado

Contents of this file

1. Introduction

2. Figures S1 to S11

Introduction

MSE, Spread and DSSS as a function of the forecast lead time: In this supplementary note, we show some figures depicting the time-evolution of the scores as a function of the forecast lead time. To recall first the definition of these scores, let's consider a dynamical system

$$\dot{\boldsymbol{x}} = \boldsymbol{f}(\boldsymbol{x}) \tag{1}$$

and a set of n ensemble forecasts $\boldsymbol{y}_{m,n}(t)$, $m = 1, \ldots, M$ performed with it, M being the size of the ensembles. If $\boldsymbol{x}_n(t)$ is the "truth" corresponding to the n^{th} forecast, then the MSE and the Spread of the forecasts are defined as

$$\text{MSE}(\tau) = \frac{1}{N} \sum_{n=1}^{N} \|\boldsymbol{x}_n(\tau) - \bar{\boldsymbol{y}}_n(\tau)\|^2$$
$$\text{Spread}^2(\tau) = \frac{1}{N} \sum_{n=1}^{N} \frac{1}{M-1} \sum_{m=1}^{M} \left\|\boldsymbol{y}_{m,n}(\tau) - \bar{\boldsymbol{y}}_n(\tau)\right\|^2$$

where

$$\bar{\boldsymbol{y}}_n(\tau) = \frac{1}{M} \sum_{m=1}^{M} \boldsymbol{y}_{m,n}(\tau)$$

is the ensemble mean over the members $\boldsymbol{y}_{m,n}(\tau)$ of the n^{th} ensemble forecast. f the Spread^2 and the MSE are close to one another, indicating that the estimated error is close to the true error, then the ensemble forecast is considered reliable (Leutbecher & Palmer, 2008). The bias-free univariate DSS for the n^{th} ensemble forecast and the i^{th} variable of the system can be written as (Siegert et al., 2019):

$$\begin{aligned}\text{DSS}_{n,i}(\tau) =& \frac{1}{2} \log(2\pi) + \frac{1}{2} \log\, \sigma_{n,i}^2(\tau) \\ &+ \frac{1}{2} \frac{M-3}{M-1} \left(\bar{y}_{n,i}(\tau) - x_{n,i}(\tau)\right)^2 \Big/ \sigma_{n,i}^2(\tau),\end{aligned}$$

where $\sigma_{n,i}^2$ is an estimator of the i^{th} variable ensemble variance:

$$\sigma_{n,i}^2(\tau) = \frac{1}{M-1} \sum_{m=1}^{M} |y_{m,n,i}(\tau) - \bar{y}_{n,i}(\tau)|^2.$$

This score can then be averaged over the N realizations:

$$\text{DSS}_i(\tau) = \frac{1}{N} \sum_{n=1}^{N} \text{DSS}_{n,i}(\tau).$$

The lower the DSS score, the more reliable the ensemble forecasts are for this particular variable.

In the context of the MAOOAM-VDDG ocean-atmosphere model considered in the paper, the Dawid-Sebastiani Score (DSS) can be aggregated per component of the system:

$$\begin{aligned}
\mathrm{DSS}_{\psi_\mathrm{a}}(\tau) &= \sum_{i=1}^{n_\mathrm{a}} \mathrm{DSS}_{\psi_{\mathrm{a},i}}(\tau) \\
\mathrm{DSS}_{\theta_\mathrm{a}}(\tau) &= \sum_{i=1}^{n_\mathrm{a}} \mathrm{DSS}_{\theta_{\mathrm{a},i}}(\tau) \\
\mathrm{DSS}_{\psi_\mathrm{o}}(\tau) &= \sum_{i=1}^{n_\mathrm{o}} \mathrm{DSS}_{\psi_{\mathrm{o},i}}(\tau) \\
\mathrm{DSS}_{\theta_\mathrm{o}}(\tau) &= \sum_{i=1}^{n_\mathrm{o}} \mathrm{DSS}_{\theta_{\mathrm{o},i}}(\tau).
\end{aligned}$$

where ψ_a and θ_a are respectively the streamfunction and temperature of the atmosphere, while ψ_o and θ_o are respectively the streamfunction and temperature of the ocean.

Finally, considering several methods to obtain the ensemble forecasts, these aggregated score can be compared to *perfect* ensemble forecasts with the Dawid-Sebastiani Skill Score (DSSS) that we defined as:

$$\begin{aligned}
\mathrm{DSSS}^{\mathrm{method}}_{\psi_\mathrm{a}}(\tau) &= 1 - \frac{\mathrm{DSS}^{\mathrm{method}}_{\psi_\mathrm{a}}(\tau)}{\mathrm{DSS}^{\mathrm{perfect}}_{\psi_\mathrm{a}}(\tau)} \\
\mathrm{DSSS}^{\mathrm{method}}_{\theta_\mathrm{a}}(\tau) &= 1 - \frac{\mathrm{DSS}^{\mathrm{method}}_{\theta_\mathrm{a}}(\tau)}{\mathrm{DSS}^{\mathrm{perfect}}_{\theta_\mathrm{a}}(\tau)} \\
\mathrm{DSSS}^{\mathrm{method}}_{\psi_\mathrm{o}}(\tau) &= 1 - \frac{\mathrm{DSS}^{\mathrm{method}}_{\psi_\mathrm{o}}(\tau)}{\mathrm{DSS}^{\mathrm{perfect}}_{\psi_\mathrm{o}}(\tau)} \\
\mathrm{DSSS}^{\mathrm{method}}_{\theta_\mathrm{o}}(\tau) &= 1 - \frac{\mathrm{DSS}^{\mathrm{method}}_{\theta_\mathrm{o}}(\tau)}{\mathrm{DSS}^{\mathrm{perfect}}_{\theta_\mathrm{o}}(\tau)}
\end{aligned}$$

The smaller the DSSS, the better. A value of zero indicates that the considered method matches the perfect ensemble reliability. On the other, a negative value of the DSSS would indicate that the method outperforms the perfect one.

We consider in this supplementary the two different model configurations mentioned in the paper, i.e. one with a weak low-frequency variability (LFV), and one with a strong LFV. In the latter case, we distinguish between two different regions of the attractor: a chaotic region for $\theta_{o,2} > 0.12$ and a more "quiet" region for $\theta_{o,2} < 0.08$.

PFMD spectra: We also plot the PFMD[1] spectra, to show that they are the same as the one obtained with DMD and depicted in the paper.

More precisely, considering two collections of states of the dynamical system (1) $\mathsf{X} = [\boldsymbol{x}_0 \dots \boldsymbol{x}_{K-1}]$ and $\mathsf{Y} = [\boldsymbol{x}_1 \dots \boldsymbol{x}_K]$, the PFMD representation of the Perron-Frobenius operator is given by

$$\mathsf{M}^{\mathrm{PFMD}} = \mathsf{A}^{\mathsf{T}}(\mathsf{G}^{+})^{\mathsf{T}}. \tag{2}$$

where $\mathsf{A} = \mathsf{Y}\mathsf{X}^{*}$ and $\mathsf{G} = \mathsf{X}\mathsf{X}^{*}$. The eigenvalues of the matrix $\mathsf{M}^{\mathrm{PFMD}}$ form then the above-mentioned spectrum.

References

Leutbecher, M., & Palmer, T. N. (2008). Ensemble forecasting. *Journal of computational physics*, *227*(7), 3515–3539.

Siegert, S., Ferro, C. A., Stephenson, D. B., & Leutbecher, M. (2019). The ensemble-adjusted Ignorance Score for forecasts issued as normal distributions. *Quarterly Journal of the Royal Meteorological Society*, *145*, 129–139.

Notes

1. PFMD for Perron-Frobenius Modes Decomposition.

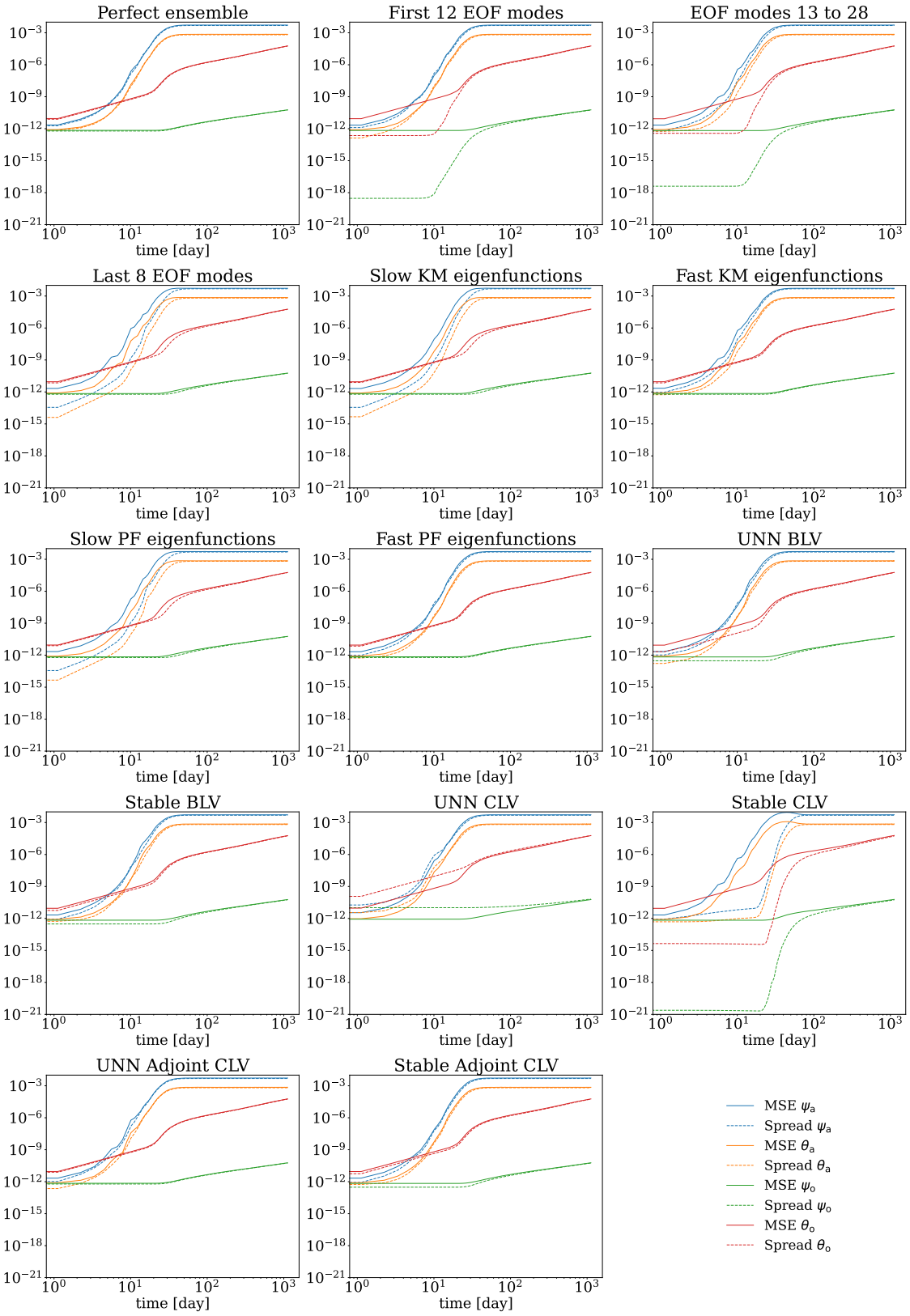

Figure S1. Experiment with the weak LFV - MSE and Spread as a function of the forecast lead time

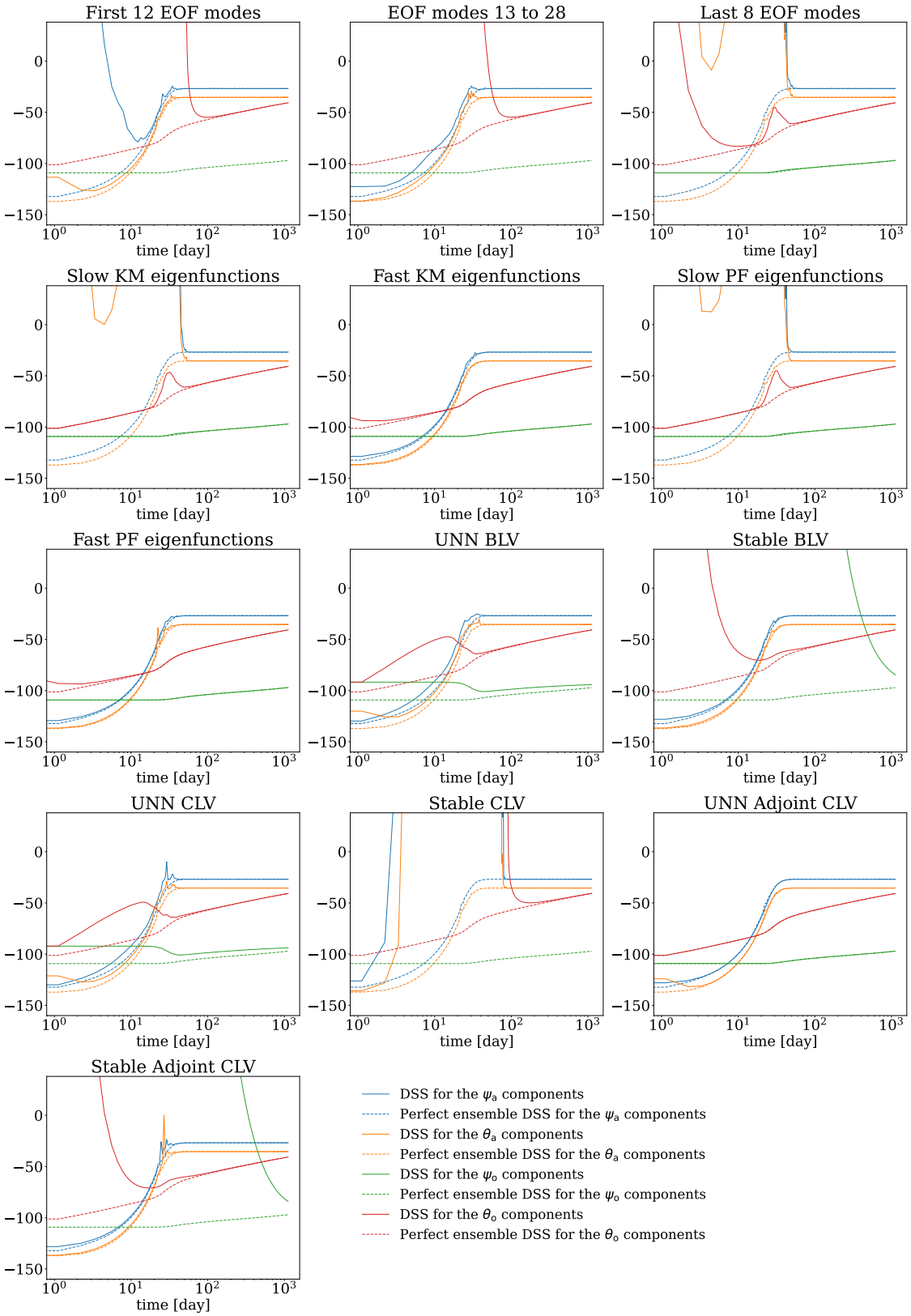

Figure S2. Experiment with the weak LFV - DSS as a function of the forecast lead time

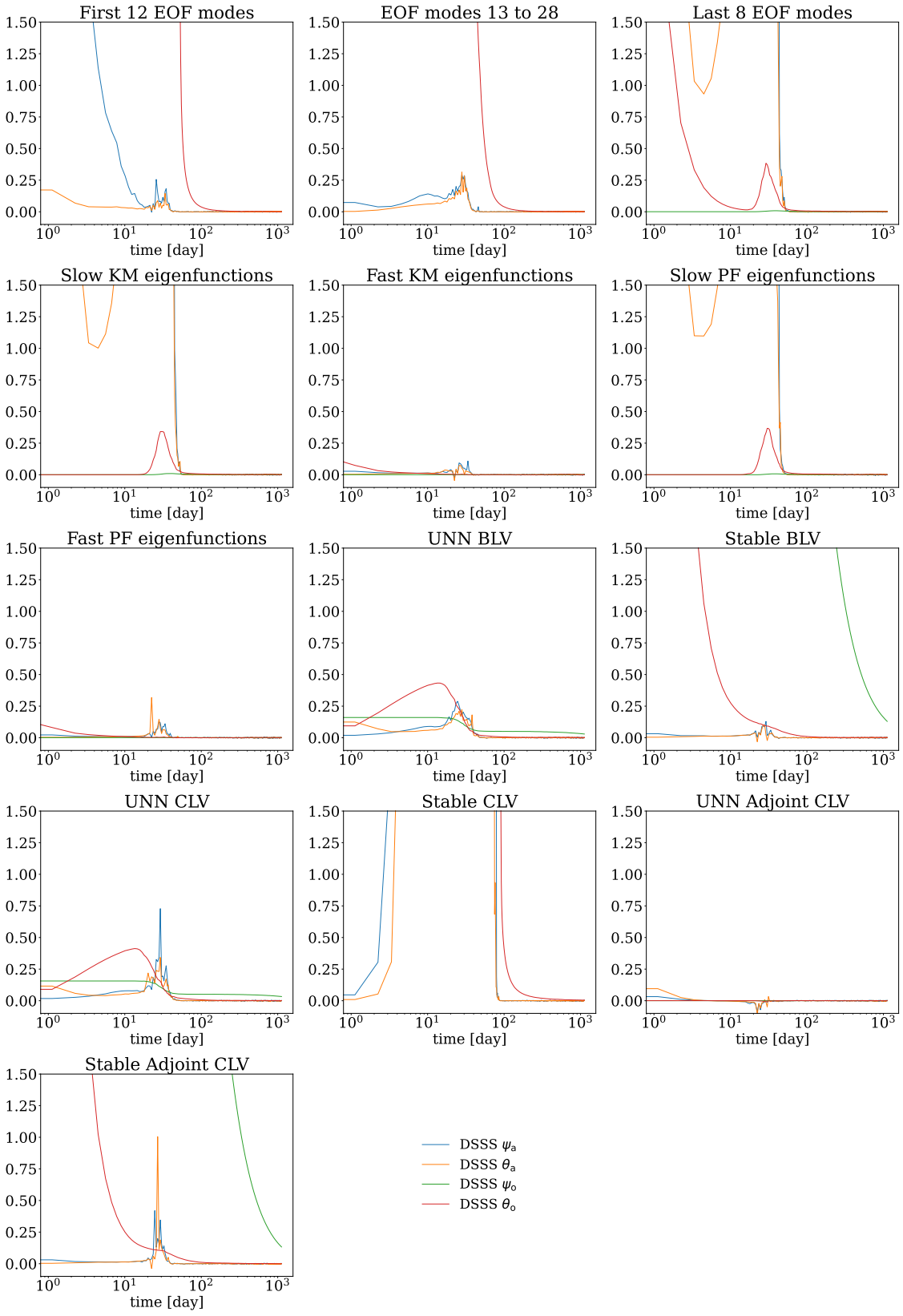

Figure S3. Experiment with the weak LFV - DSSS as a function of the forecast lead time

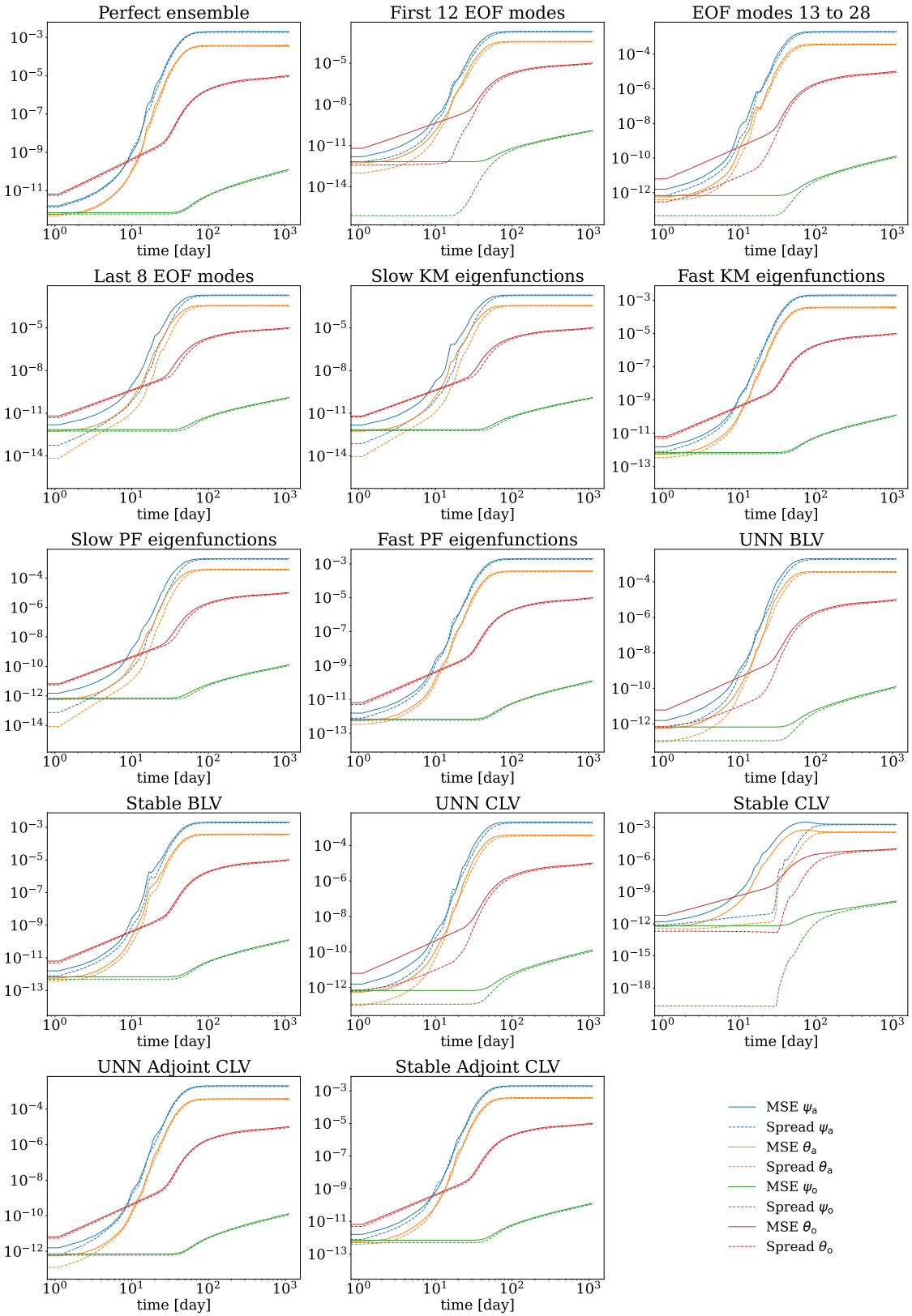

Figure S4. Experiment with the strong LFV, case where $\theta_{o,2} > 0.12$ - MSE and Spread as a function of the forecast lead time

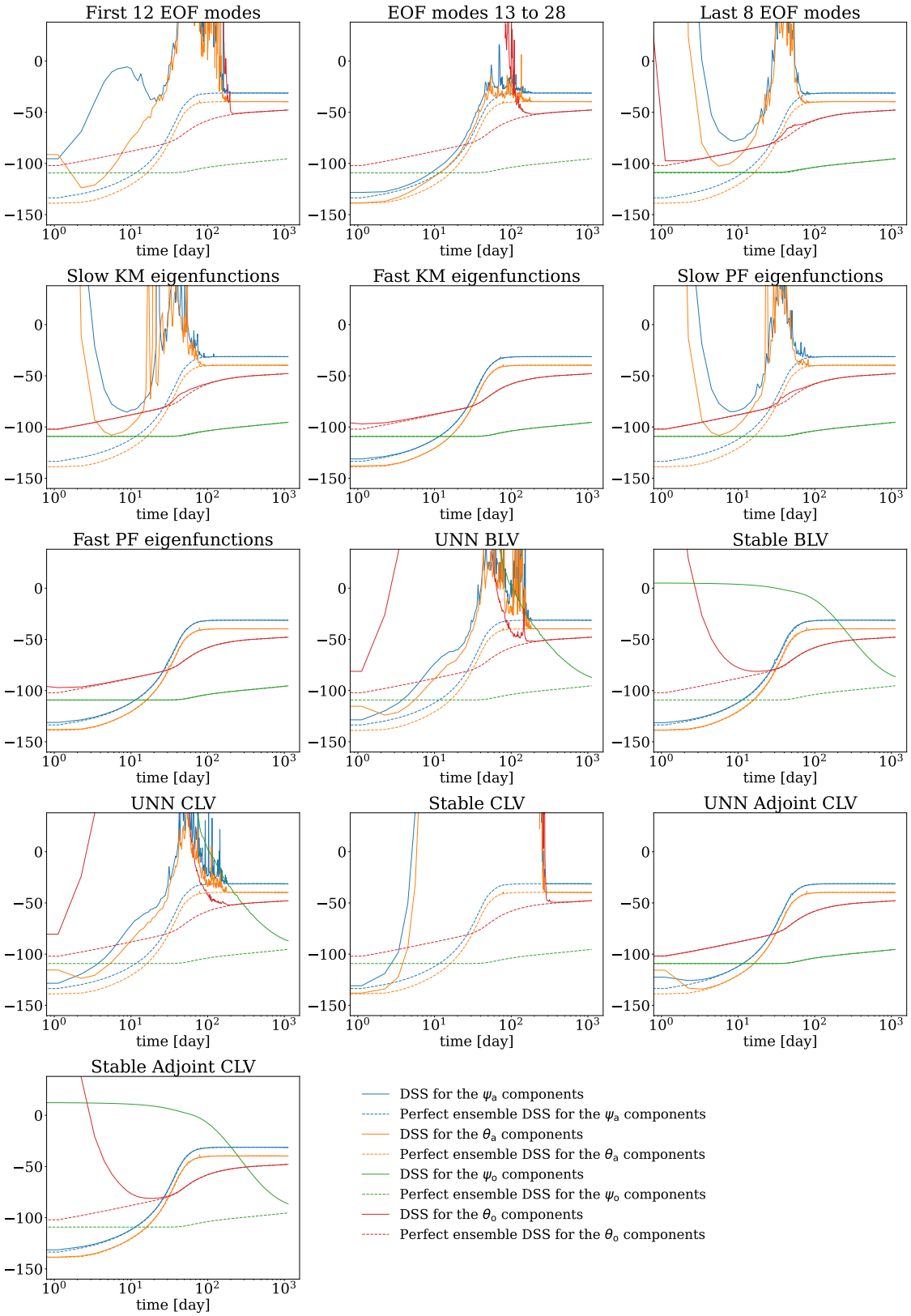

Figure S5. Experiment with the strong LFV, case where $\theta_{o,2} > 0.12$ - DSS as a function of the forecast lead time

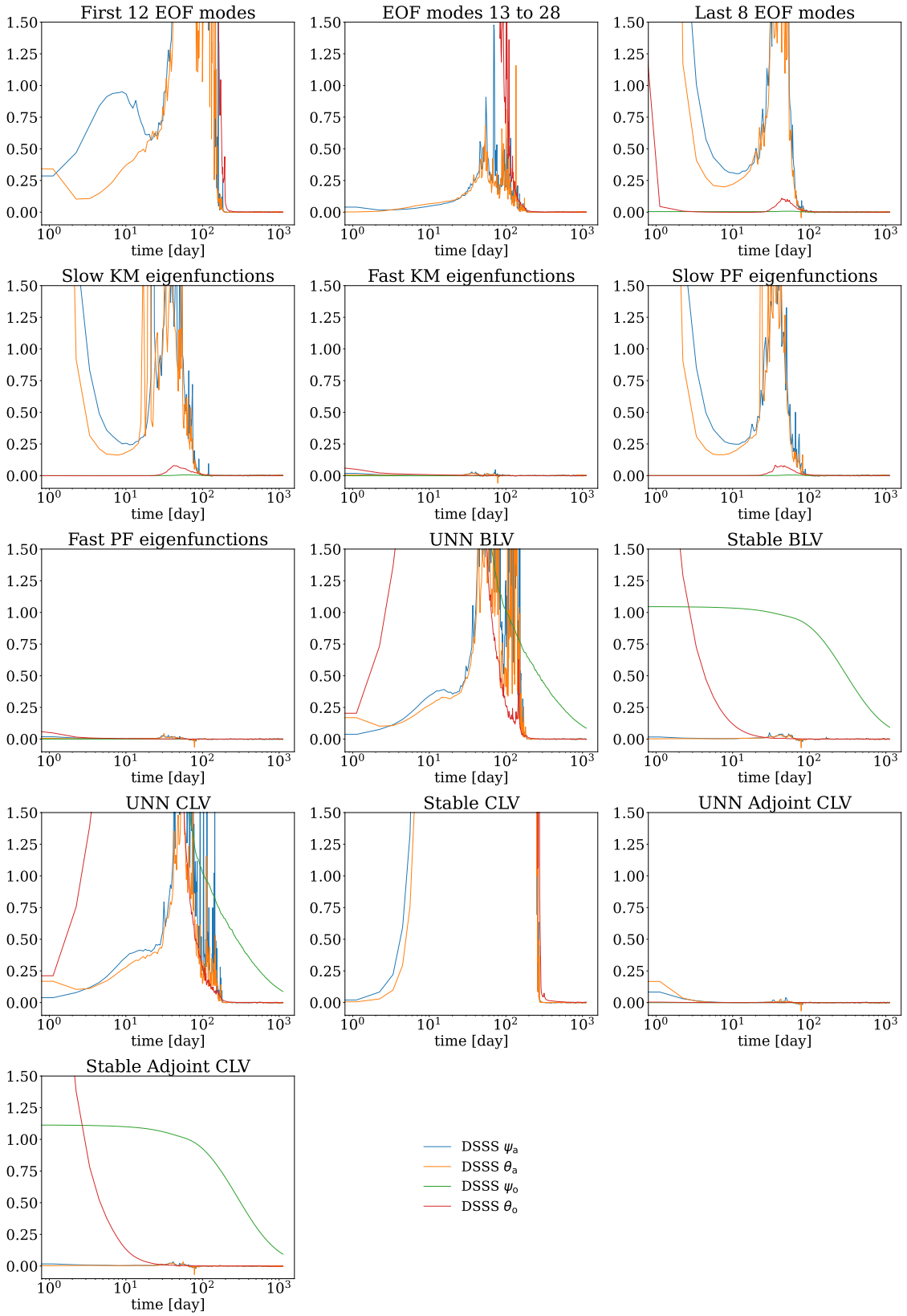

Figure S6. Experiment with the strong LFV, case where $\theta_{o,2} > 0.12$ - DSSS as a function of the forecast lead time

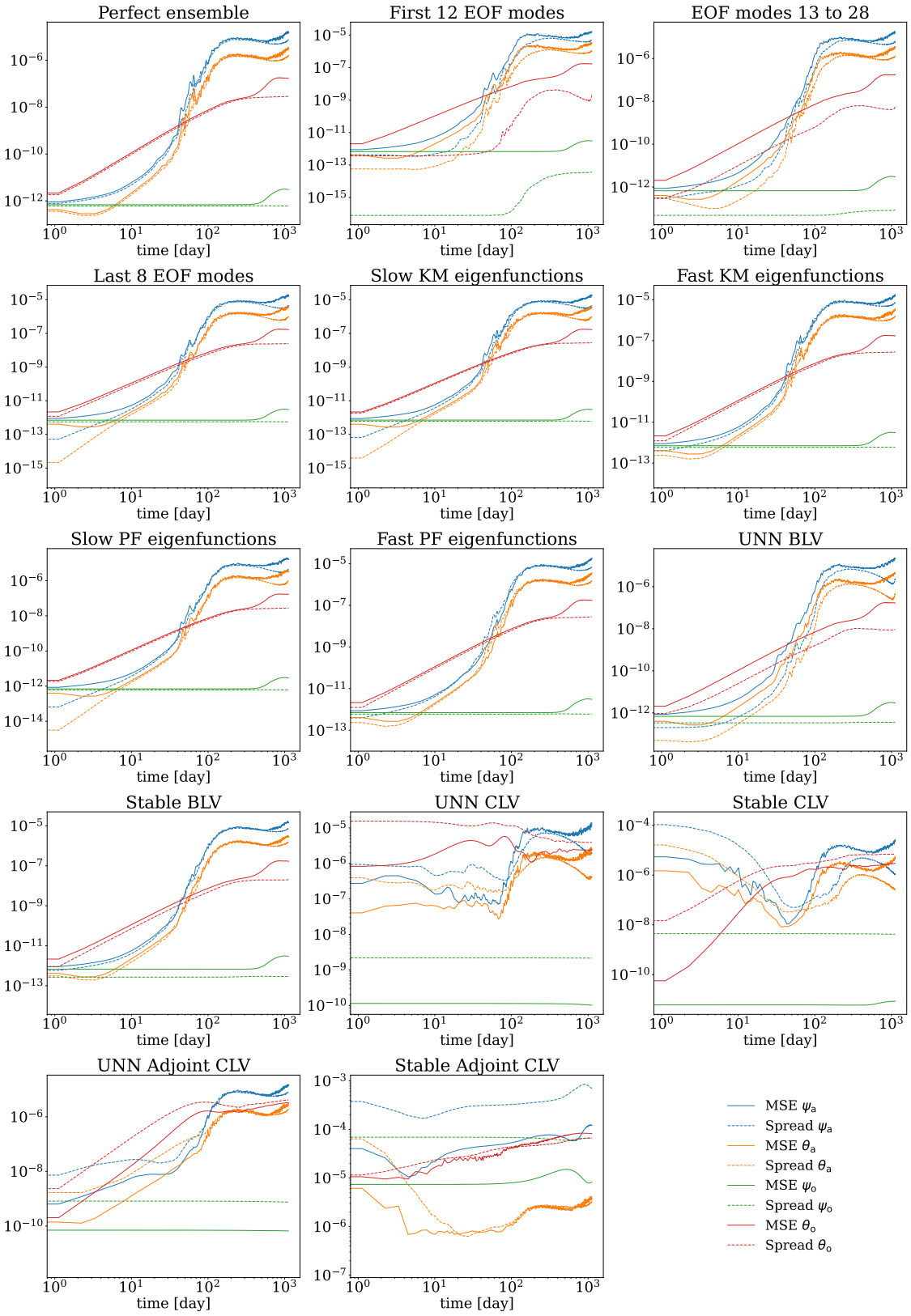

Figure S7. Experiment with the strong LFV, case where $\theta_{o,2} < 0.08$ - MSE and Spread as a function of the forecast lead time

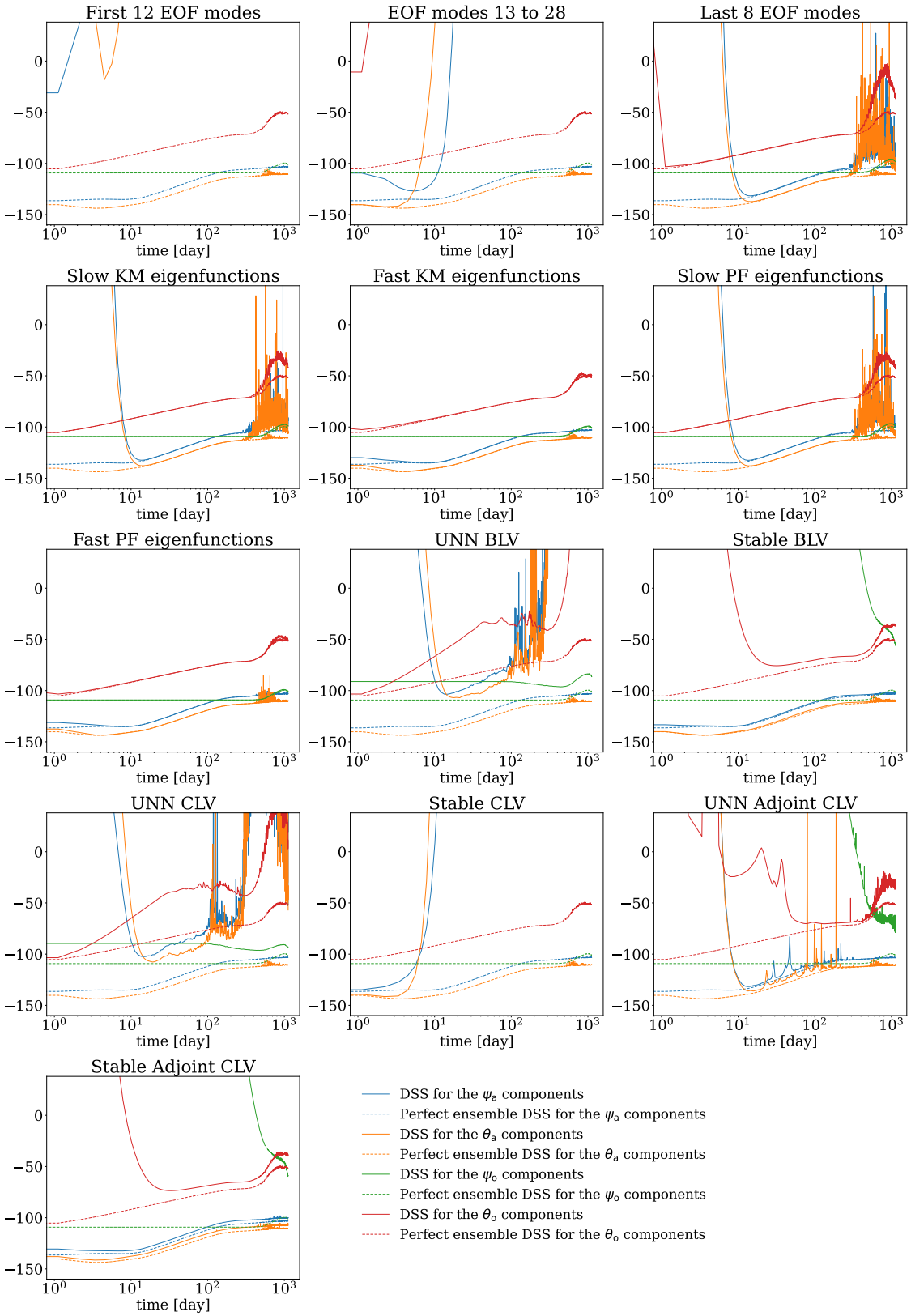

Figure S8. Experiment with the strong LFV, case where $\theta_{o,2} < 0.08$ - DSS as a function of the forecast lead time

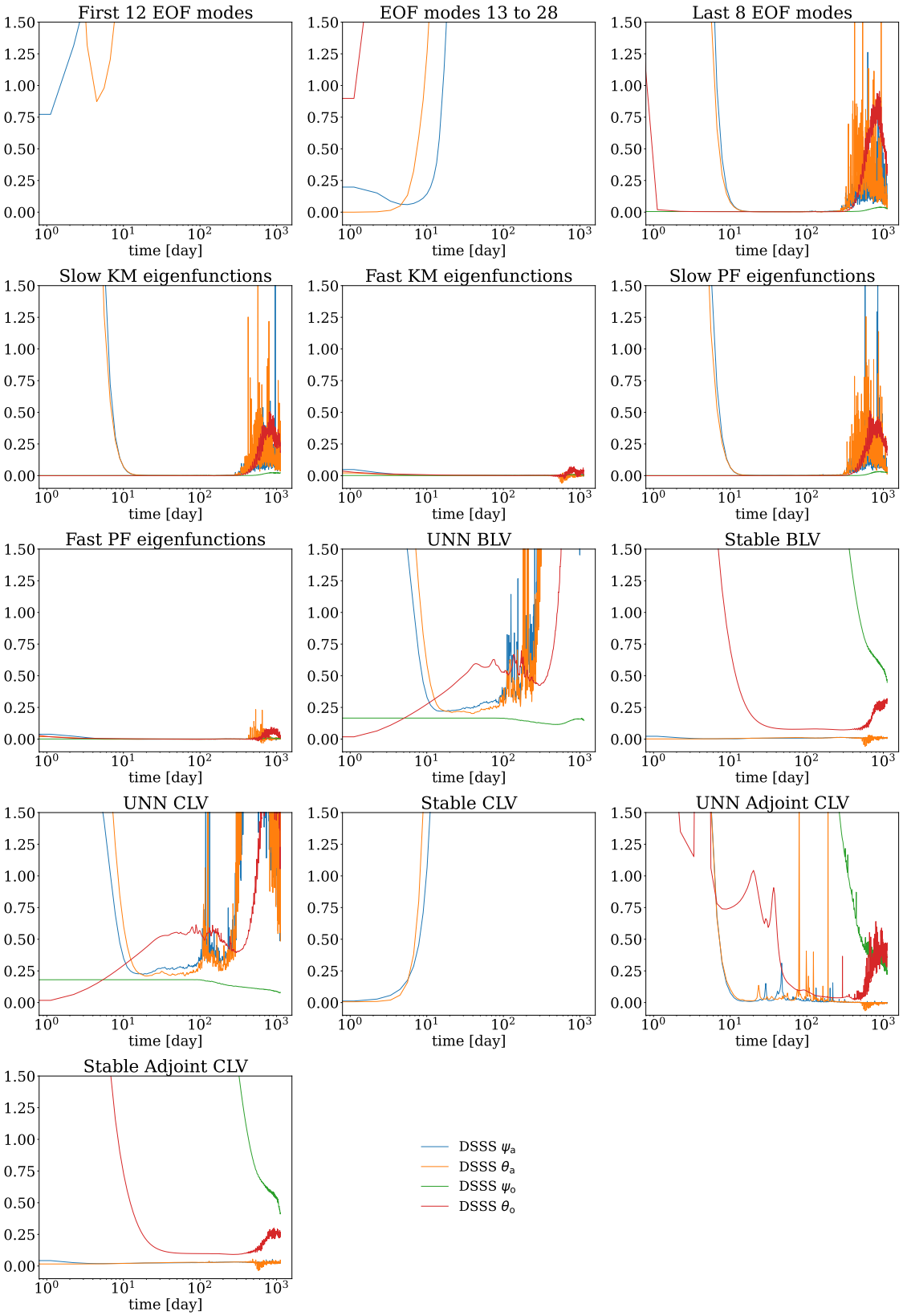

Figure S9. Experiment with the strong LFV, case where $\theta_{o,2} < 0.08$ - DSSS as a function of the forecast lead time

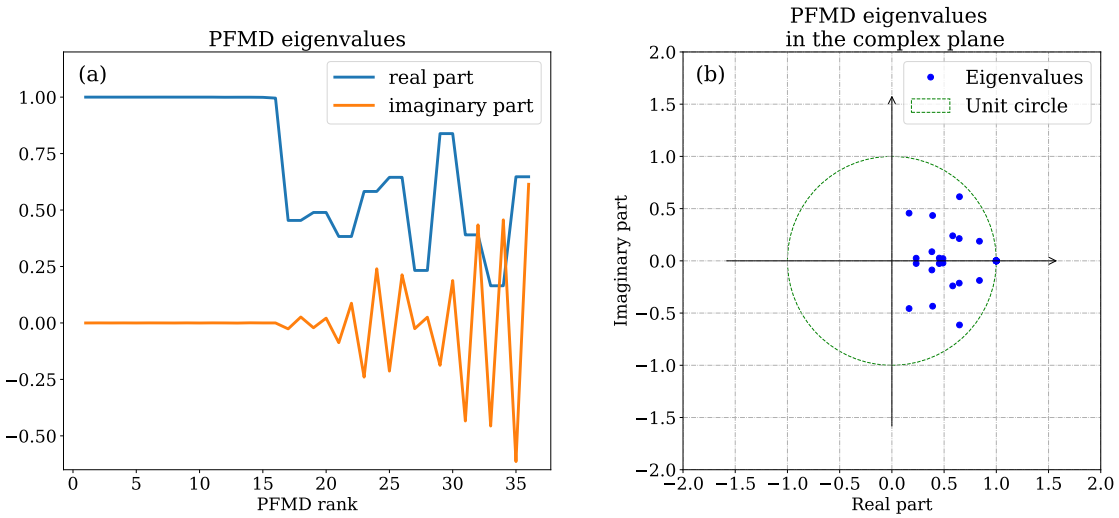

Figure S10. Experiment with the weak LFV - PFMD spectra

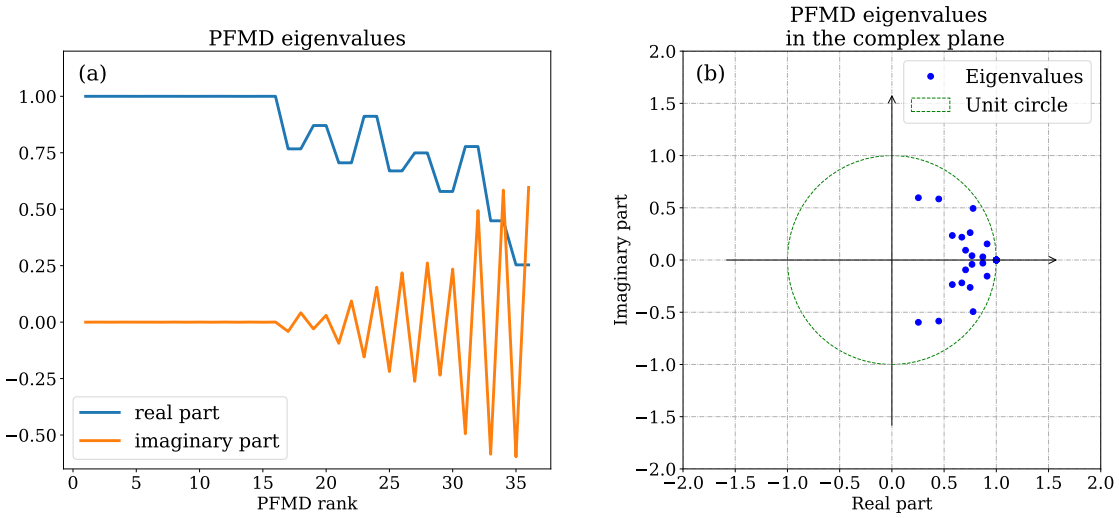

Figure S11. Experiment with the strong LFV - PFMD spectra